ACS SyntheticBiology

pubs.acs.org/synthbio

Research Article

Systematic Engineering of *Synechococcus elongatus* UTEX 2973 for Photosynthetic Production of L-Lysine, Cadaverine, and Glutarate

Zachary A. Dookeran and David R. Nielsen*

Cite This: *ACS Synth. Biol.* 2021, 10, 3561−3575

Read Online

ACCESS | Metrics & More | Article Recommendations | Supporting Information

ABSTRACT: Amino acids and related targets are typically produced by well-characterized heterotrophs including *Corynebacterium glutamicum* and *Escherichia coli*. Cyanobacteria offer an opportunity to supplant these sugar-intensive processes by instead directly utilizing atmospheric CO_2 and sunlight. *Synechococcus elongatus* UTEX 2973 (hereafter UTEX 2973) is a particularly promising photoautotrophic platform due to its fast growth rate. Here, we first engineered UTEX 2973 to overproduce L-lysine (hereafter lysine), after which both cadaverine and glutarate production were achieved through further pathway engineering. To facilitate metabolic engineering, the relative activities of a subset of previously uncharacterized promoters were investigated, in each case, while also comparing the effects of both chromosomal (from neutral site NS3) and episomal (from pAM4788) expressions. Using these parts, lysine overproduction in UTEX 2973 was engineered by introducing a feedback-resistant copy of aspartate kinase (encoded by $lysC^{fbr}$) and a lysine exporter (encoded by *ybjE*), both from *E. coli*. While chromosomal expression resulted in lysine production up to just 325.3 ± 14.8 mg/L after 120 h, this was then increased to 556.3 ± 62.3 mg/L via plasmid-based expression, also surpassing prior reports of photoautotrophic lysine bioproduction. Lastly, additional products of interest were then targeted by modularly extending the lysine pathway to glutarate and cadaverine, two 5-carbon, bioplastic monomers. By this approach, glutarate has so far been produced at final titers reaching 67.5 ± 2.2 mg/L by 96 h, whereas cadaverine has been produced at up to 55.3 ± 6.7 mg/L. Overcoming pathway and/or transport bottlenecks, meanwhile, will be important to improving upon these initial outputs.

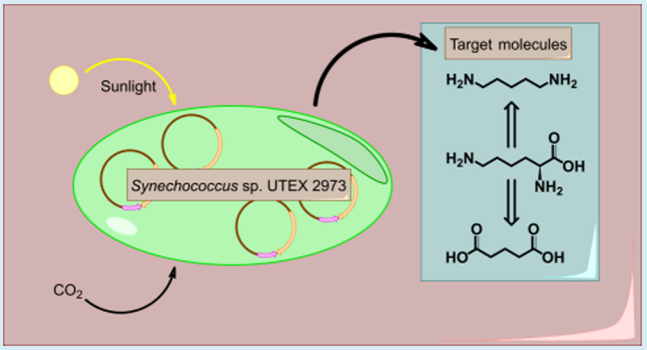

KEYWORDS: *Synechococcus elongatus UTEX 2973, lysine, cadaverine, glutarate*

INTRODUCTION

Lysine is a proteinogenic amino acid that is produced industrially at a rate of over 2.5 million tons per year[1] (with an annual growth of roughly 7%[2]) and which serves as an important nutritional supplement, poultry and fish feed additive,[2] and key ingredient in the production of cosmetics and pharmaceuticals.[3,4] Meanwhile, in addition to representing a valuable product itself, lysine can furthermore serve as a precursor to other useful building-block chemicals. For example, lysine can be enzymatically converted to each of cadaverine (a diamine),[5−7] 5-aminovalerate (AMV; an ω-amino acid), or glutarate (a dicarboxylate),[8−10] all of which can serve as monomers for the production of biobased plastics. Currently, most lysine is produced fermentatively by strains of *Corynebacterium glutamicum*, a Gram-positive heterotroph that has served as an industrial workhorse for amino acid biosynthesis since its discovery in 1957.[11,12] Moving beyond classical mutagenesis techniques, the more recent rational engineering of genetically defined *C. glutamicum* strains[13−18] has enabled the bioproduction of lysine at final titers of up to 221 ± 18 g/L and productivities as high as 5.5 g/(L h).[19] Despite such impressive performance, this current production route relies solely upon the provision of sugar feedstocks (e.g., glucose, fructose, and sucrose from starches, raw sugar, and molasses), the likes of which directly compete with food supplies.[20−23]

In contrast to the conventional production of lysine (and its derived chemicals) from sugars, a promising alternative instead involves the use of photoautotrophic biocatalysts, which use light for energy and atmospheric CO_2 as the sole carbon source, an approach that circumvents the food cycle and offers the potential to reduce atmospheric CO_2 release/accumulation. To this end, Korosh and colleagues were the first to report on the photosynthetic production lysine using engineered cyanobacteria.[24] In this case, using the model

Received: October 2, 2021
Published: December 1, 2021

https://doi.org/10.1021/acssynbio.1c00492
ACS Synth. Biol. 2021, 10, 3561−3575

Table 1. List of Plasmids Constructed and Used in This Study to Characterize the Relative Behaviors of Different Expression Control Systems in UTEX 2973

plasmid	genotype
pZD-LGC-01	pANS; *yemGFP*-T_{rrnB2}; Km^R
pZD-LGC-02	pANS; P_{cpcB1*}–*yemGFP*-T_{rrnB2}; Km^R
pZD-LGC-03	pANS; P_{J23119}–*yemGFP*-T_{rrnB2}; Km^R
pZD-LGC-04	pANS; P_{trc2O}–*yemGFP*-T_{T7}–P_{MB2}-*lacI*^{WF}; Km^R
pZD-LGC-05	pANS; P_{conII}–Riboswitch-F–*yemGFP*-T_{T7}–P_{MB2}-*lacI*^{WF}; Km^R
pZD-LGC-06	NS3::P_{tac}–*yemGFP*-T_{rrnB2}; Km^R
pZD-LGC-07	NS3::*yemGFP*-T_{rrnB2}; Km^R
pZD-LGC-08	NS3::P_{cpcB1*}–*yemGFP*-T_{rrnB2}; Km^R
pZD-LGC-09	NS3::P_{J23119}–*yemGFP*-T_{rrnB2}; Km^R
pZD-LGC-10	NS3::P_{trc2O}–*yemGFP*-T_{T7}–P_{MB2}-*lacI*^{WF}; Km^R
pZD-LGC-11	NS3::P_{conII}–Riboswitch-F–*yemGFP*-T_{T7}-*lacI*^{WF}; Km^R

Table 2. List of Plasmids Constructed and Used in This Study to Engineer the Production and/or Export of Lysine, Cadaverine, and Glutarate

plasmid	genotype
pZD-LGC-13	NS3::P_{trc2O}–*lysC*^{fbr}-T_{T7}–P_{MB2}-*lacI*^{WF}; P_{cpcB1*}–*ybjE*-T_{psbC}; Km^R
pZD-LGC-14	pANS; P_{trc2O}–*lysC*^{fbr}-T_{T7}–P_{MB2}-*lacI*^{WF}; Km^R
pZD-LGC-15	pANS; P_{cpcB1*}–*ybjE*-T_{rrnB2}; Km^R
pZD-LGC-16	pANS; P_{trc2O}–*yemGFP*-T_{T7}–P_{MB2}-*lacI*^{WF}; P_{cpcB1*}–*ybjE*-T_{psbC}; Km^R
pZD-LGC-17	pANS; P_{trc2O}–*lysC*^{fbr}-T_{T7}–P_{MB2}-*lacI*^{WF}; P_{cpcB1*}–*ybjE*-RBS_{cpcA1}–*yemGFP*-T_{psbC}; Km^R
pZD-LGC-18	pANS; P_{trc2O}–*lysC*^{fbr}-T_{T7}–P_{MB2}-*lacI*^{WF}; P_{cpcB1*}–*ybjE*-RBS_{cpcA1}–*pck*-T_{psbC}; Km^R
pZD-LGC-19	pANS; P_{trc2O}–*lysC*^{fbr}-T_{T7}–P_{MB2}-*lacI*^{WF}; P_{cpcB1*}–*ybjE*-RBS_{cpcA1}–*ppc*-T_{psbC}; Km^R
pZD-LGC-20	pANS; P_{trc2O}–*lysC*^{fbr}-T_{T7}–P_{MB2}-*lacI*^{WF}; P_{cpcB1*}–*ybjE*-RBS_{cpcA1}–*pyc*-T_{psbC}; Km^R
pZD-LGC-21	pANS; P_{trc2O}–*lysC*^{fbr}-T_{T7}–P_{MB2}-*lacI*^{WF}; P_{cpcB1*}–*ybjE*-P_{J23119}–*pyc*-T_{psbC}; Km^R
pZD-LGC-22	pANS; P_{cpcB1*}–*cgmA*-T_{psbC}; Km^R
pZD-LGC-23	pANS; P_{cpcB1*}–*sapBCDF*-T_{psbC}; Km^R
pZD-LGC-24	pANS; P_{J23119}–*cadB*-T_{rrnB2}; Km^R
pZD-LGC-25	pANS; P_{trc2O}–*lysC*^{fbr}-T_{T7}–P_{MB2}-*lacI*^{WF}; P_{cpcB1*}–*ybjE*-RBS_{cpcA1}–*cadB*-T_{psbC}; Km^R
pZD-LGC-26	pANS; P_{cpcB1*}–*ybjE*-RBS_{cpcA1}–*cadB*-T_{psbC}; Km^R
pZD-LGC-27	pANS; P_{cpcB1*}–*ybjE*-P_{J23119}–*cadB*-T_{psbC}; Km^R
pZD-LGC-28	pANS; P_{trc2O}–*lysC*^{fbr}-T_{rrnB}-T_{T7}–P_{MB2}-*lacI*^{WF}; P_{cpcB1*}–*ybjE*-T_{psbC}; Km^R
pZD-LGC-29	pANS; P_{conII}–Riboswitch-F–*cadA*-T_{T7}–P_{MB2}-*lacI*^{WF}; Km^R
pZD-LGC-30	pANS; P_{trc2O}–*lysC*^{fbr}-T_{rrnB}–P_{conII}–Riboswitch-F–*cadA*-T_{T7}–P_{MB2}-*lacI*^{WF}; P_{cpcB1*}–*sapBCDF*-T_{psbC}; Km^R
pZD-LGC-31	pANS; P_{trc2O}–*lysC*^{fbr}-T_{T7}–P_{MB2}-*lacI*^{WF}; P_{cpcB1*}–*ybjE*-RBS_{cpcA1}–*davDT*-T_{psbC}; Km^R
pZD-LGC-32	pANS; P_{trc2O}–*lysC*^{fbr}-T_{T7}–P_{MB2}-*lacI*^{WF}; P_{cpcB1*}–*davBA*-RBS_{cpcA1}–*davDT*-T_{psbC}; Km^R
pZD-LGC-33	pANS; P_{trc2O}–*lysC*^{fbr}-T_{T7}–P_{MB2}-*lacI*^{WF}; P_{cpcB1*}–*davBA*-P_{J23119}–*davDT*-T_{psbC}; Km^R

marine cyanobacterium *Synechococcus* sp. PCC 7002 (hereafter PCC 7002), key pathway bottlenecks were overcome by (i) expressing a heterologous and feedback deregulated copy of aspartate kinase and (ii) introducing a heterologous lysine exporter. The resulting strain was ultimately able to produce up to 455 mg/L-lysine after 20 days. Although an impressive titer, the volumetric productivity, in this case, reached a maximum of just 3 mg/(L h). As lysine biosynthesis is inherently coupled with growth, we hypothesized that its photosynthetic production could be enhanced by instead employing a faster-growing cyanobacterium as the host platform. Notably, in contrast to PCC 7002, whose doubling time has been reported as 4.1 h,[25] UTEX 2973—a freshwater cyanobacterium related to both *S. elongatus* PCC 6301 and PCC 7942—has a doubling time as fast as just 1.5 h under optimal conditions.[26] UTEX 2973 has also shown the potential to serve as a robust host for engineering the photosynthetic production of various biochemicals. For example, UTEX 2973 has previously been used to express the entire 42 kb hapalindole synthesis pathway of *Fischerella ambigua* UTEX 1903.[27] Moreover, UTEX 2973 has also proven to be a prodigious host for sugar biosynthesis, achieving a maximum titer of 8.7 g/L sucrose over 21 days of continuous production,[28] before then ultimately achieving a maximal sucrose productivity of 1.1 g/(L day) through additional engineering.[29] Finally, UTEX 2973 has also recently been engineered for the photosynthetic production of limonene[30] at up to 16.4 mg/L and a rate (8.2 mg/(L day)) roughly 8-fold greater than that reported for previously engineered (and slower growing) cyanobacterial species.

In this study, we first sought to engineer UTEX 2973 to overproduce lysine by analogously deregulating the main pathway bottleneck and introducing a heterologous exporter. These efforts, along with the final bioproduction performance, were aided via the characterization of a subset of versatile promoter systems as well as a novel episomal expression strategy. Lysine-producing UTEX 2973 was then subsequently leveraged to investigate the biosynthesis of both cadaverine and glutarate, two bioplastic monomers whose direct photosynthetic production has not before been reported.

https://doi.org/10.1021/acssynbio.1c00492
ACS Synth. Biol. 2021, 10, 3561−3575

MATERIALS AND METHODS

Chemicals. All enzymes were purchased from New England Biolabs (Ipswich, MA). Cadaverine (>98%) was purchased from TCI America (Portland, OR). All other chemicals were purchased at the highest available purities from Sigma-Aldrich (St. Louis, MO) or Santa Cruz Biotechnology (Dallas, TX), unless otherwise indicated.

Strains and Culture Conditions. UTEX 2973 was obtained from the UTEX Culture Collection of Algae at the University of Texas at Austin. Culturing in liquid media and on solid agar plates was performed using BG-11 medium buffered with 10 mM triethylsilane (TES)/NaOH, pH 8.2 (where agar plates were also supplemented with 3 g/L sodium thiosulfate) at 38 °C under continuous light at an intensity of ∼200 μmol photon m^{-2} s^{-1}, unless otherwise specified. Where necessary, plasmids were maintained in UTEX 2973 via the addition of 50 μg/mL kanamycin. Liquid cultures were grown while shaking at 200 rpm in 250 mL nonbaffled flasks containing 25 mL media after being seeded to an initial cell density as determined by the optical density at 750 nm (OD_{750}) of 0.1. Growth at 1% CO_2 was carried out in a Caron Plant Growth Chamber Model 7300 (Marietta, OH) set to maximum humidity (∼63%). An example of the typical growth profile of wild-type UTEX 2973 under these conditions can be seen in Figure S1. Where appropriate, the expression of relevant pathway genes via the inducible P_{trc2O}-*lacI*/O and P_{conII}–Riboswitch-F systems was achieved by the addition of isopropyl-β-D-1-thiogalactopyranoside (IPTG) (at up to 500 μM) and/or theophylline (at up to 2 mM), respectively.

Plasmid Construction. All plasmids constructed and/or used for gene expression in this study are summarized in Tables 1 and 2. All plasmids constructed for this study were assembled via the Gibson assembly method.[31] All oligonucleotide primers used in plasmid assembly and sequencing were custom-designed and then synthesized by IDT (Coralville, IA) and are listed in Table S1. Plasmid pCDF-*lysC*^{fbr}–dapA^{fbr} served as the template for the feedback-resistant (fbr) copy of aspartate kinase (encoded by *lysC*^{fbr}), originally derived from *E. coli* MG1655.[8] *E. coli* MG1655 genomic DNA (gDNA) served as the template for genes encoding the lysine exporter (*ybjE*), cadaverine antiporter (*cadB*), phosphoenolpyruvate carboxykinase (*pck*), the phosphoenolpyruvate carboxylase (*ppc*), the cadaverine export system (*sapBCDF*), and lysine decarboxylase (*cadA*). *C. glutamicum* ATCC 13032 gDNA served as the template for genes encoding pyruvate carboxylase (*pyc*), cadaverine exporter (*cgmA*), and dicarboxylic acid exporter (*ynfM*). *Pseudomonas putida* KT2440 gDNA served as the template for the native operons encoding lysine 2-monooxygenase and 5-aminopentanamidase (*davBA*) as well as glutarate-semialdehyde dehydrogenase and 5-aminovalerate aminotransferase (*davDT*). Plasmid pSL3137 served as the template for the P_{trc2O} promoter and the T_{rrnB} terminator.[32] Plasmid pCMJ049 served as the template for T_{T7}-P_{MB2}-*lacI*^{WF}, used in the construction of all IPTG-inducible expression cassettes.[33] UTEX 2973 gDNA served as the template for the P_{cpcB1*} promoter and the T_{psbC} terminator, as well as the upstream and downstream regions of the NS3 neutral site. The shuttle vector pAM4788-Km^R was constructed by amplifying and assembling together a fragment from pAM4788 of *S. elongatus* sp. PCC 7942,[34] with one containing the Km^R cassette from pEERM1.[35] All plasmids were screened first by colony PCR, followed by restriction digest mapping and final verification via DNA sequencing.

Genetic Modification of UTEX 2973. All constructed shuttle and integration vectors were delivered to UTEX 2973 via conjugation, in this case, using a tripartite mating procedure adapted from Yu and colleagues.[25] Briefly, UTEX 2973 was inoculated in 50 mL BG-11 media (as described above), while two strains of *E. coli*—DH5α, harboring the conjugal plasmid pRL443, and DH5α MCR, harboring both the helper plasmid pRL623 and the desired cargo plasmid—were simultaneously inoculated into separate tubes containing 5 mL Luria broth (LB) media with appropriate antibiotics. Following overnight growth, by which time UTEX 2973 had reached approximately early-exponential phase (OD_{750} = 0.4–0.8), both *E. coli* cultures were pelleted by centrifugation at 3000*g* for 5 min before then decanting the supernatant and resuspending each pellet in 5 mL fresh LB media containing no antibiotics. This procedure was repeated twice more. Meanwhile, UTEX 2973 was harvested by pelleting at 2000*g* for 10 min, before decanting the supernatant and resuspending the cells in 5 mL of fresh BG-11. In a sterile 1.5 mL tube, 250 μL of resuspended DH5α carrying pRL443 was then mixed with 250 μL of resuspended DH5α MCR carrying pRL623 and the cargo plasmid. Next, 500 μL of resuspended UTEX 2973 was added to the same tube, after which it was then tightly capped and inverted several times to mix. Following this, 200 μL of the tripartite mating mixture was pipetted directly onto a BG-11 + 5% LB agar plate containing no antibiotics, spread evenly across the face of the agar using glass beads, and then allowed to air-dry. The plate was then incubated as described above, except that light intensity was set to 10–40 μmol photon m^{-2} s^{-1}. After 16–24 h, a sterile metal spatula was used to separate and lift the BG-11 agar from the Petri dish to allow 600 μL fresh BG-11 liquid media with kanamycin to be pipetted into the bottom of the dish (i.e., below the agar). The agar was then reseated into the Petri dish, allowing kanamycin to diffuse through the agar where it would reach an approximate final concentration of 50 μg/mL. Exconjugants typically appeared after 3–4 days, at which point they were picked and streaked onto a fresh BG-11 plate containing 50 μg/mL kanamycin.

Fluorescence Measurements. Relative expression levels by different constructs were determined by measuring differences in whole-cell fluorescence of *yemGFP*-expressing strains (prepared via the same growth and induction conditions described above) 12 h after inoculation (i.e., early to mid-exponential phase). At this point, OD_{750} was measured (which ranged from 0.3 to 0.7) and 100 μL of culture was transferred to a 96-well black-bottom Costar plate. Fluorescence was then measured using an Infinite M Nano+ Tecan microplate reader, where the excitation and emission wavelengths were set to 489 and 520 nm, respectively. Raw fluorescence data were then normalized by OD_{750}.

Sample Preparation for Intracellular Metabolite Analysis. Select metabolites of interest were assayed with respect to their intracellular accumulation by first harvesting cells by centrifugation at 3000*g* for 5 min, before then resuspending and washing the pellet three times using the same volume of sterile deionized water to remove any extracellular products. The final cell pellet was then stored at −80 °C overnight before being dried via lyophilization (Labconco FreeZone 2.5, LABCONCO). Fully dried pellets were weighed and then lysed using Bugbuster Master Mix solution (Novagen), with samples being incubated on a

https://doi.org/10.1021/acssynbio.1c00492
ACS Synth. Biol. 2021, 10, 3561–3575

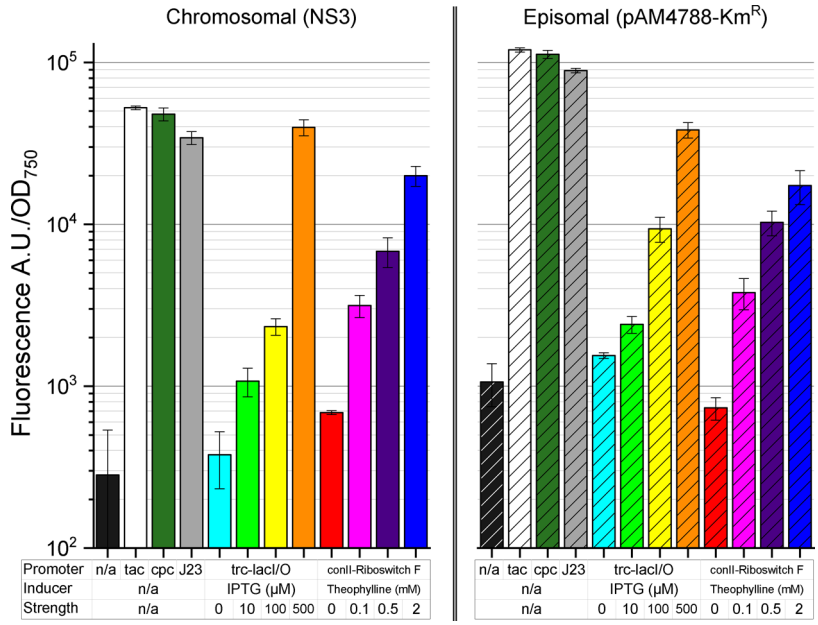

Figure 1. Characterization of the relative behaviors of different expression control systems and the influence of their chromosomal versus episomal application. Arbitrary fluorescence units normalized by OD_{750} for different promoters and a riboswitch when chromosomally integrated at NS3 (left, solid bars) or expressed on the self-replicating plasmid pAM4788-Km^R (right, striped bars) into UTEX 2973. The tested systems include no promoter (control; charcoal); tac promoter (white); cpcB1* promoter (denoted as "cpc", dark green); J23119 promoter (denoted as "J23", gray); the P_{trc2O}-*lacI*/*O* system with 0 μM (cyan), 10 μM (bright green), 100 μM (yellow), and 500 μM IPTG (orange); and P_{conII}−Riboswitch-F with 0 mM (red), 0.1 mM (pink), 0.5 mM (purple), and 2.0 mM theophylline (blue). Error bars represent standard error from biological triplicate.

shaking platform at room temperature for 20 min. Following centrifugation of lysed samples at 12 000*g* for 20 min, 30 μL of the clarified solution was derivatized for analysis, as described below.

Quantification of UTEX 2973 Growth. Cell growth was measured by OD_{750} using a Thermo Spectronic BioMate 3 UV−vis spectrophotometer and correlated with dry cell weight (DCW). To do so, three flasks of wild-type UTEX 2973 were cultured as described above, with cell biomass being harvested at different time points during exponential growth. Cells were concentrated by centrifugation, washed, dried by lyophilization (as above), and weighed. The resulting correlation is shown in Figure S2.

Metabolite Quantification. Periodically throughout each culture, aqueous samples were removed for amino acid analysis via high-performance liquid chromatography (HPLC) following a diethyl ethoxymethylenemalonate (DEEMM) derivatization method adapted from that of Kim and colleagues.[36] First, 50 μL of culture was centrifuged at 12 000*g* for 10 min to remove cells (note: an equal volume of fresh BG-11 medium buffered with 10 mM TES/NaOH, pH 8.2 was then added back to the culture to maintain a constant volume). Next, 30 μL of the resulting supernatant was added to an HPLC sample vial containing 189 μL deionized water, 18 μL of 0.5 M borate buffer solution (pH 9.0; Alfa Aesar), 60 μL methanol, and 3 μL DEEMM. The vial was then tightly capped and allowed to stand at room temperature for 2 h before analysis. Analysis was carried out using an Agilent 1100 Series HPLC equipped with a diode array detector set to 284 nm. The derivatized sample (5 μL) was injected and separated using an Agilent Hypersil GOLD C18 column (4.6 ×250 mm, 5 μm particle size) maintained at 35 °C using a mobile phase flowing at 1 mL/min and consisting of acetonitrile (A) and 25 mM aqueous sodium acetate buffer, pH 4.8 (B) according to the following gradient program: 0−2 min, 20−25% A; 2−32 min, 25−60% A; 32−40 min, 60−20% A. Under these conditions, L-aspartate (aspartate hereafter), 5-aminovalerate (5-AMV), lysine, and cadaverine eluted at 3.6, 9.3, 12.7, and 26.3 min, respectively. For each analyte of interest, authentic standards were used to prepare solutions of known concentrations, after which they were each identically derivatized to generate their respective external calibration curves.

Where appropriate, culture samples were also analyzed for glutarate via HPLC. In this case, 250 μL culture was collected, cells were removed by pelleting, and 200 μL of supernatant was then added to a HPLC vial containing 200 μL deionized water. Analysis was carried out using the above instrument; however, analytes were detected via a refractive index detector maintained at 35 °C. Moreover, in this case, separation was performed using a Bio-Rad Aminex HPX-87H column (7.8 mm×300 mm, 9 μm particle size) maintained at 35 °C and a mobile phase consisting of 5 mM H_2SO_4 at a constant flow rate of 0.77 mL/min. Under these conditions, glutarate eluted at 11.0 min. An external calibration curve for glutarate was also generated using solutions prepared from an authentic standard.

RESULTS

Expanding the Portfolio of Genetic Parts for Metabolic Engineering of UTEX 2973. Despite its promising phenotypic traits, and in contrast to both commonly employed heterotrophic chasses (e.g., *E. coli*, *C. glutamicum*) and even other more established cyanobacterial strains (e.g., PCC 7002, *Synechocystis* sp. PCC 6803), UTEX 2973 currently suffers from a relative shortage of well-characterized genetic parts, which, in turn, limits metabolic engineering efforts. However, since the genome of UTEX 2973 differs from that of its parent PCC 7942 by just 55 single nucleotide polymorphisms and indels,[25] this has fortuitously enabled a range

https://doi.org/10.1021/acssynbio.1c00492
ACS Synth. Biol. 2021, 10, 3561−3575

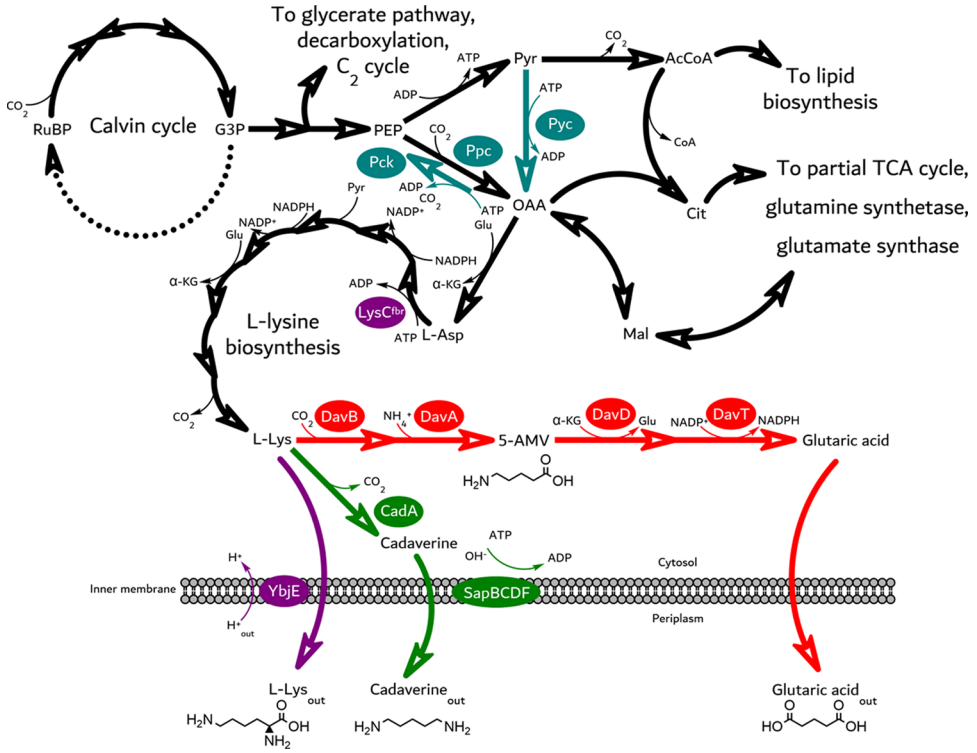

Figure 2. Lysine production in UTEX 2973 and engineered pathways to cadaverine and glutarate, encompassing central carbon metabolism, lysine biosynthesis, and the introduction of heterologous genes. Genes overexpressed to increase lysine production, and export genes are shown in purple, including *lysC*^{fbr}, feedback-resistant aspartate kinase, and *ybjE*, lysine exporter. Genes overexpressed to increase the production of oxaloacetate (OAA) are shown in teal, including *pck*, pyruvate carboxykinase; *ppc*, phosphoenolpyruvate carboxylase; and *pyc*, pyruvate carboxylase. Cadaverine production genes are shown in dark green and include *cadA*, lysine decarboxylase; and *sapBCDF*, polyamine exporter. Glutarate production genes are shown in red and include *davB*, lysine 2-monooxygenase; *davA*, 5-aminopentanamidase; *davD*, glutarate-semialdehyde dehydrogenase; and *davT*, 5-aminovalerate aminotransferase. Metabolites shown include RuBP, RuBisCO; G3P, glyceraldehyde 3-phosphate; PEP, phosphoenolpyruvate; Pyr, pyruvate; AcCoA, acetyl-coenzyme A; Cit, citrate; OAA, oxaloacetic acid; Mal, malate; L-Asp, aspartate; L-Lys, lysine; and 5-AMV, 5-aminovalerate.

of promoters and other translational control systems to be effectively ported over.[27,37] That said, it has also been previously shown (e.g., in the case of P_{psbA} from *Amaranthus hybridus* chloroplasts) that relative promoter strengths can be quite variable between UTEX 2973[37] and PCC 7942.[38] Moreover, genetic parts can often also display context-dependent activities, including with respect to the specific expression site employed.[35] In UTEX 2973, most part characterization has to date been confined to one of either neutral site NS1[39] or NS2.[40] Finally, although copy number variation has been shown to hold an outsized influence over total gene expression levels in other microorganisms,[41−43] its relative influences have yet to be thoroughly examined in UTEX 2973 due to the lack of an available self-replicating shuttle vector. With these limitations in mind, we first sought to characterize the relative activities of a tractable subset of promoters and a riboswitch from both the less commonly employed neutral site NS3,[44] as well as the as-yet-unexplored (to the best of our knowledge) pAM4788 shuttle vector (derived from the endogenous pANS small plasmid of PCC 7942).[34] The pAM4788 plasmid is particularly promising for this purpose as its included toxin−antitoxin system has been reported to facilitate its stable maintenance for up to at least 5 weeks, even in the absence of antibiotic selection.[34]

We first constructed and confirmed that pAM4788-Km^R could be transformed into and stably maintained in UTEX 2973 (Supporting Information Figure S3), a largely expected result since UTEX 2973 also carries the pANS small plasmid and it is identical to the copy from PCC 7942.[34] Next, *yemGFP* production levels were compared for a small subset of gene expression systems to characterize their relative strengths under both chromosomal (NS3) and episomal (pAM4788-Km^R) conditions. As seen in Figure 1, all of the tested systems were found to be functional from both loci, including the constitutive P_{tac}, P_{cpcB1*}, and P_{J22119} promoters, as well as the IPTG-inducible P_{trc2O}-*lacI*/O promoter system and the theophylline-inducible P_{conII}−Riboswitch-F, with the latter two uniquely providing titratable control as a function of inducer concentration. Overall, while chromosomal expression provided a higher dynamic range than episomal expression (roughly 186- vs 113-fold), the highest overall levels of *yemGFP* production were seen in the latter case (Figure 1). For example, using P_{tac} (originally present on pAM4788-Km^R), roughly 2.3-fold higher normalized fluorescence levels were achieved when *yemGFP* was expressed from pAM4788-Km^R vs NS3. A similar magnitude of difference was also observed in the case of P_{cpcB1*}. Although this ratio could be taken to reflect the relative pAM4788-Km^R versus chromosome copies in UTEX 2973, it is notably less than the reported ratio (of about 10) for pANS in PCC 7942.[34] Meanwhile, although similar maximum expression levels were achieved for the inducible P_{trc2O}-*lacI*/O system at the highest IPTG induction level (i.e., 500 μM IPTG) under both chromosomal and episomal conditions, at all lower induction levels, at least a 2.2-fold

https://doi.org/10.1021/acssynbio.1c00492
ACS Synth. Biol. 2021, 10, 3561−3575

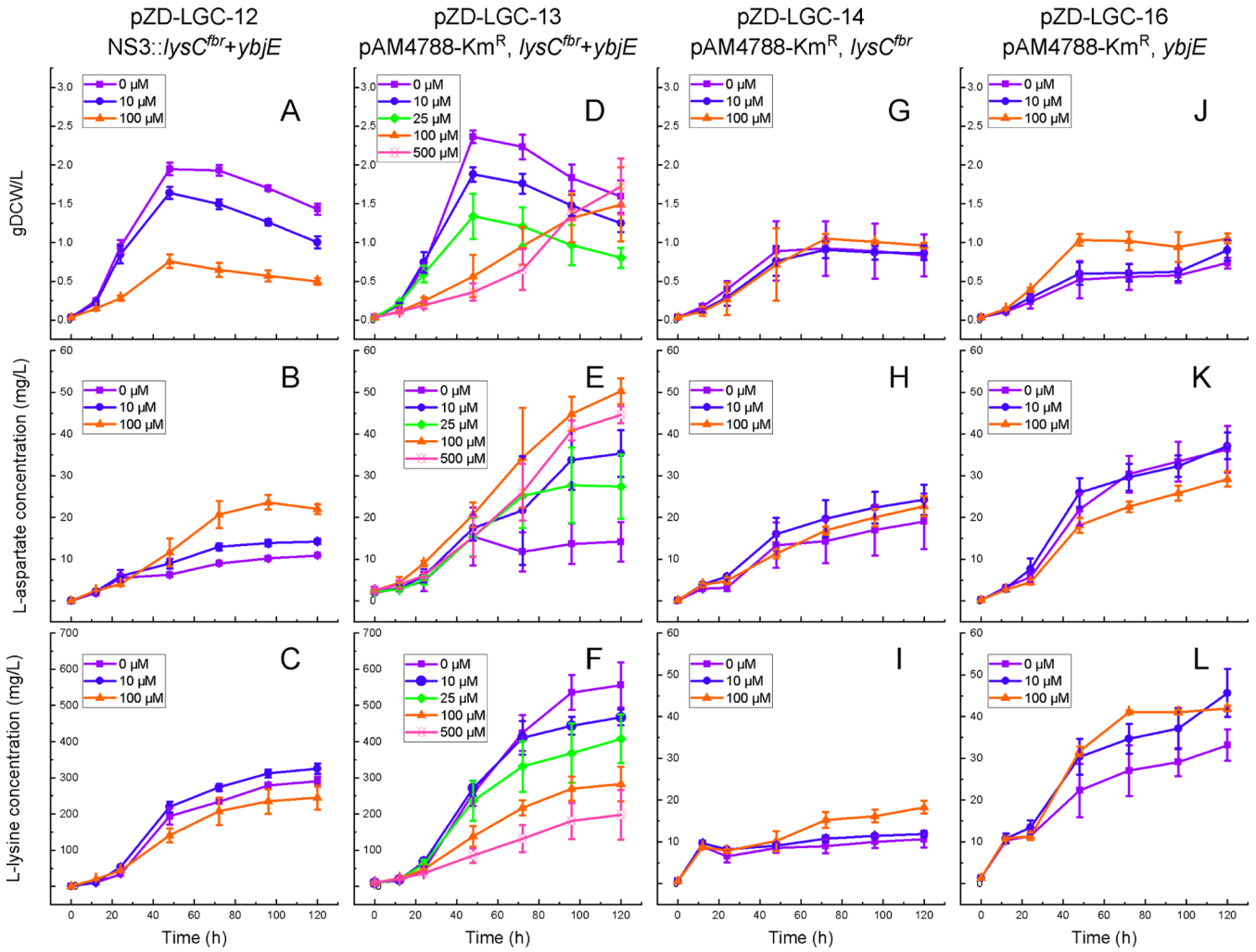

Figure 3. Comparison of lysine production via chromosomal and episomal pathway expression in UTEX 2973. Comparing cell growth (top row), extracellular aspartate accumulation (middle row), and extracellular lysine accumulation (bottom row) by engineered UTEX 2973 strains over the course of 120 h when grown in shake flasks containing 25 mL BG-11 and varying concentrations of IPTG. From left column to right: strains conjugated with pZD-LGC-12 for the chromosomal expression of *lysC*^{fbr} + *ybjE* (A–C), pZD-LGC-13 for the episomal expression of *lysC*^{fbr} + *ybjE* (D–F), pZD-LGC-14 for the episomal expression of *lysC*^{fbr} (G–I), and pZD-LGC-15 for the episomal expression of *ybjE* (J–L). IPTG concentrations used were 0 μM (purple squares), 10 μM (blue circles), 25 μM (green diamonds), 100 μM (orange triangles), and 500 μM (pink bullseye). Error bars represent standard error from biological triplicate.

difference was again observed. Furthermore, in the absence of IPTG, a statistically significant increase in fluorescence relative to the no promoter control was only observed in the episomal case, suggesting that higher gene copy number also increased the net effect of "leaky" expression (i.e., a less tight OFF state). In contrast, meanwhile, statistically significant differences in chromosomal vs episomal *yemGFP* expression via the P_{conII}–Riboswitch-F system were only observed at 0.5 mM theophylline (where the difference was still only <2-fold). This result is consistent with past reports where, as observed for other RNA-based genetic switches, regulation has predominantly been shown to be controlled by the concentration of the conformation-changing molecule (i.e., inducer) and not mRNA abundance.[45−47] Importantly, this behavior also resulted in the P_{conII}–Riboswitch-F providing the tightest OFF state when employed on pAM4788-Km^R, with fluorescence levels being indistinguishable from even the no promoter control. The opposite was also true, however, when the P_{conII}–Riboswitch-F was used on the chromosome, with higher levels of fluorescence being observed relative to both the no promoter control and the P_{trc2O}-*lacI*/O system in the absence of IPTG. Overall, where the dynamic (i.e., inducible) control of expression is needed in UTEX 2973, these findings indicate a trade-off between a tight OFF state and overall expression, both of which benefited from the increased copy number provided by episomal expression, though in an opposite manner between the two expression systems examined. Lastly, although there is no guarantee that the pathway genes of interest will be expressed at a strength equivalent to *yemGFP*, these characterized parts at least provide a useful starting point for making relative comparisons while optimizing each pathway.

Engineering UTEX 2973 for Lysine Overproduction. Equipped with the above-characterized parts and following the general metabolic engineering template first established in PCC 7002 by Korosh et al.,[24] we next sought to engineer UTEX 2973 for lysine overproduction by (i) relieving allosteric inhibition caused by lysine upon aspartate kinase and (ii) enhancing lysine export (Figure 2). Plasmid pZD-LGC-12 was accordingly constructed by cloning *lysC*^{fbr} under control of the

https://doi.org/10.1021/acssynbio.1c00492
ACS Synth. Biol. 2021, 10, 3561−3575

IPTG-inducible P_{trc2O}-*lacI*/O promoter system and *ybjE* under control of the strong and constitutive P_{cpcB1*} promoter. Homology arms surrounding the cassette were also included to enable integration into NS3. Once fully segregated, the resulting strain (UTEX 2973 NS3::*lysC*^{fbr} + *ybjE*) was tested for its ability to overproduce lysine by culturing it at different IPTG induction levels (0, 10, or 100 μM; Figure 3C). Ultimately, maximum production was achieved using 10 μM IPTG where, after 120 h, the final lysine titer reached 325.3 ± 14.8 mg/L. At 100 μM IPTG, meanwhile, biomass levels were significantly reduced (Figure 3A). In all cases, despite generally increasing lysine titers over the entire culture duration, cell density declined as cultivation continued past 48 h. For example, even at the optimal level of 10 μM IPTG, although the culture reached a maximum biomass density of 1.64 ± 0.08 g-DCW/L by 48 h, it ultimately fell to 1.00 ± 0.08 g-DCW/L by the end of the culture (120 h). For comparison, wild-type UTEX 2973 under the same conditions does not typically exhibit such a collapse (Figure S1), suggesting that this behavior indeed results as a consequence of lysine overproduction.

The observation that excessive *lysC*^{fbr} expression (i.e., >10 mM IPTG) negatively impacted both growth and lysine production could suggest that increased competition for aspartate (the immediate precursor to lysine) and/or its central metabolic precursor oxaloacetate (OAA) was responsible. However, in addition to growth and lysine production losses, increased *lysC*^{fbr} expression was actually found to correspond with a greater extracellular accumulation of aspartate (Figure 3B). Notably, in addition to supporting the lowest lysine titer, the highest *lysC*^{fbr} induction level (i.e., 100 μM IPTG) also yielded the most aspartate, reaching 22.0 ± 1.2 mg/L by 120 h, roughly 2-fold higher than with 10 μM IPTG. As this would seemingly suggest that essential precursors were not critically drained, it seems more plausible that, as demonstrated in other bacteria, the negative effects of high *lysC*^{fbr} induction are instead associated with a more generalized disruption of a stringently regulated amino acid network.[13,24]

Lastly, it is noted that this initial strain employing chromosomal coexpression of *lysC*^{fbr} and *ybjE* represents a design analogous to the PCC 7002-derived lysine overproducer developed by Korosh and colleagues.[24] For comparison, under its own unique optimal expression conditions, that strain was capable of producing up to 254.4 ± 17.5 mg/L-lysine by 96 h (in this case using standard media A$^+$, 1% CO_2, and ∼200 μmol photon m^{-2} s^{-1}), which is slightly below the 312.3 ± 10.9 mg/L produced here in the same time by UTEX 2973 NS3::*lysC*^{fbr} + *ybjE*. Thus, the average volumetric productivity here was increased by 41% (3.8 vs 2.7 mg/(L h)) as a result of alternatively employing fast-growing UTEX 2973. Indeed, the initial volumetric growth rate (i.e., over the first 48 h) of UTEX 2973 NS3::*lysC*^{fbr} + *ybjE* was nearly 2-fold faster than that of the PCC 7002 lysine overproducer under the respective conditions examined, reaching an average of 34 mg-DCW/(L h). That said, the PCC 7002 lysine overproducer did not display the same decline in biomass as observed here (i.e., beyond 48 h), suggesting that unknown genotypic differences were responsible. This is further reflected by the fact that, while maximal lysine production by UTEX 2973 required low and optimized *lysC*^{fbr} expression, maximal expression was instead required in PCC 7002. Although differences in expression systems surely played a role (in PCC 7002, *lysC*^{fbr} was expressed via the tetracycline-inducible P_{EZtet} promoter), we hypothesize that key central metabolic differences between UTEX 2973 and PCC 7002 also contributed to the contrasting phenotypes. In particular, while there is no known α-ketoglutarate dehydrogenase encoded in cyanobacterial genomes[48] (responsible for converting α-ketoglutarate to succinyl-CoA as part of a complete TCA cycle[49]), individual cyanobacteria address this void in different ways.[50] For instance, *Synechocystis* sp. PCC 6803 maintains a functional γ-aminobutyric acid (GABA) shunt,[51] whereas PCC 7002 utilizes α-ketoglutarate decarboxylase and succinic semialdehyde dehydrogenase in the absence of 2-oxoglutarate dehydrogenase.[52,53] The situation is furthermore different in UTEX 2973, as genes associated with both such routes are missing and thus so is its ability to operate a complete TCA cycle. Instead, past labeling data suggest that UTEX 2973 may use a linear pathway to convert OAA to citrate and α-ketoglutarate and, furthermore, converts a portion of aspartate to fumarate (via *RS11515* and *RS01375*, which can then be converted to the TCA organic acids malate and succinate) via purine metabolism.[54] These differences may increase the sensitivity of UTEX 2973 to changes in its endogenous OAA and aspartate pools and, as such, also the confound influence of increased aspartate kinase activity, which, in turn, may impose greater stress on central carbon metabolism relative to PCC 7002.

Enhancing Lysine Production via Episomal Pathway Expression. To improve upon the performance of UTEX 2973 NS3::*lysC*^{fbr} + *ybjE*, we next sought to investigate if an episomal expression strategy could instead be employed to increase lysine production, ideally while reducing (or eliminating) the need to supply costly IPTG. A single cassette featuring P_{trc2O}−*lysC*^{fbr}-T_{T7}−P_{MB2}-*lacI*^{WF} and P_{cpcB1*}−*ybjE*-T_{psbC} was cloned from pZD-LGC-12 and into the pAM4788-Km^R shuttle vector, resulting in pZD-LGC-13. UTEX 2973 harboring pZD-LGC-13 was then analogously cultivated under a range of IPTG concentrations (Figure 3D−F). As expected, the episomal expression of *lysC*^{fbr} reduced the requirement for IPTG induction, with maximal lysine production now occurring in its complete absence (i.e., "leaky expression" by the P_{trc2O}-*lacI*/O system). In this case, the maximal lysine titer was increased to 556.3 ± 62.3 mg/L after 120 h, a 71% improvement relative to UTEX 2973 NS3::*lysC*^{fbr} + *ybjE* with 10 μM IPTG. As before, increasing beyond the optimal IPTG level reduced both growth and lysine production as well as resulted in the increased accumulation of aspartate, in this case reaching a maximum of 50.3 ± 3.1 mg/L at 100 μM IPTG. Furthermore, a prolonged lag phase also emerged at IPTG concentrations above 25 μM, likely as a result of excessive metabolic burden.

We lastly sought to examine if lysine production could be further improved by increasing metabolite flux toward OAA, thereby providing a greater "push" into the lysine pathway. Pyruvate carboxykinase (encoded by *pck*) and phosphoenolpyruvate carboxylase (encoded by *ppc*) from *E. coli* as well as pyruvate carboxylase (encoded by *pyc*) from *C. glutamicum* are all central metabolic enzymes whose overexpression has been extensively examined in heterotrophs as a means to boost the production of various biochemicals derived from OAA[19,55] (Figure 2). Among these, Pyc notably catalyzes the direct conversion of pyruvate to OAA; a reaction not known to natively occur in UTEX 2973. Each of *pck*, *ppc*, and *pyc* was individually coexpressed alongside *lysC*^{fbr} and *ybjE* to examine their potential effect on photosynthetic lysine production.

https://doi.org/10.1021/acssynbio.1c00492
ACS Synth. Biol. 2021, 10, 3561−3575

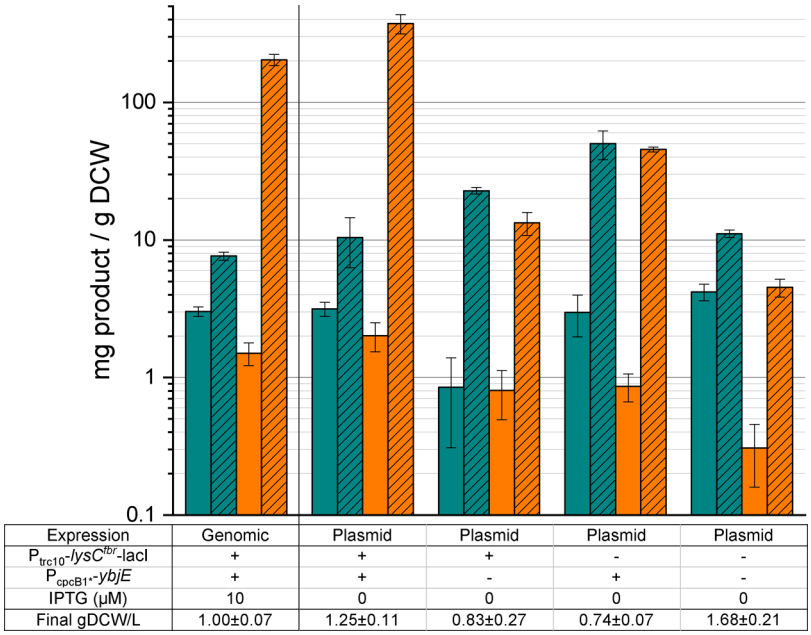

Expression	Genomic	Plasmid	Plasmid	Plasmid	Plasmid
P_{trc10}-*lysC*^{fbr}-lacI	+	+	+	-	-
P_{cpcB1*}-*ybjE*	+	+	-	+	-
IPTG (μM)	10	0	0	0	0
Final gDCW/L	1.00±0.07	1.25±0.11	0.83±0.27	0.74±0.07	1.68±0.21

Figure 4. Comparison of intracellular versus extracellular lysine accumulation by different UTEX 2973 mutants. Intracellular (solid bars) and extracellular (striped bars) concentrations of aspartate (teal) and lysine (orange) were determined per unit biomass for selected UTEX 2973 mutants after 120 h. Error bars represent standard error from biological triplicate.

However, as seen in Supporting Information Figure S4, in all cases, the maximum final lysine titers were reduced relative to UTEX 2973 harboring pZD-LGC-13 (by 23.6−55.2%). Though unsuccessful for improving lysine production, this outcome reinforces the past observation that, in UTEX 2973, native PEP carboxylase already drives significant flux to OAA,[54] which places additional importance on *lysC*^{fbr} as the pathway bottleneck rather than another upstream step.

Confirming the Importance of *lysC*^{fbr} and *ybjE* Coexpression. While the results thus far have confirmed that the general metabolic engineering strategy developed previously for PCC 7002[24] was sufficient and similarly effective for engineering lysine overproduction by UTEX 2973, the essentiality of *lysC*^{fbr} and/or *ybjE* overexpression for achieving this phenotype was not yet explicitly determined. Although aspartate kinase has been predicted in UTEX 2973 (encoded by *RS11150*), its regulatory behavior and potential role as a pathway bottleneck have not yet been investigated. Meanwhile, although there are currently only three known lysine-specific exporters, including *YbjE* from *E. coli*,[56] *LysE* from *C. glutamicum*,[57−59] and the recently discovered *MglE* from *Xenopus oocyte*,[60] none show significant homology with any protein in UTEX 2973 and no other native lysine exporters have otherwise been identified (directly or inferred). Accordingly, a series of control strains were constructed to individually examine the roles and importance of both *lysC*^{fbr} and *ybjE* expression on lysine production in UTEX 2973. As seen in Figure 3G−I, when *lysC*^{fbr} alone was episomally expressed via P_{trc2O}-*lacI*/O (using pZD-LGC-14) with up to 100 μM IPTG, both cell growth (reaching a maximum of 1.05 ± 0.06 g-DCW/L by 72 h) and lysine production (reaching a maximum of just 18.3 ± 1.5 mg/L by 120 h) were significantly reduced. Thus, with lysine export being significantly disrupted in the absence of *ybjE* coexpression, its intracellular accumulation was likely responsible for the significant fitness defect. Meanwhile, when *ybjE* alone was episomally expressed via P_{cpcB1*} (pZD-LGC-16), both cell growth (peaking at 1.05 ± 0.06 g-DCW/L by 120 h) and lysine production (reaching just 45.7 ± 5.8 mg/L by 120 h) were again similarly reduced (note: IPTG was added to maintain identical culture conditions; Figure 3J−L). Furthermore, this strain also secreted and accumulated significant levels of aspartate, reaching as high as 37.1 ± 3.2 mg/L, an observation that may suggest that *ybjE* itself displays some activity on aspartate. Reduced fitness in this case, meanwhile, was likely instead due to export losses of a more limited endogenous lysine pool. Lastly, the function and importance of *ybjE* (as well as other factors) were further examined by analyzing the constructed strains with respect to changes in intra- vs extracellular levels of lysine and aspartate (both on a per-cell-mass basis) following 120 h of culturing (Figure 4). While levels of intracellular lysine remained relatively constant across all strains expressing either *lysC*^{fbr} or *ybjE* (∼0.8−2.1 mg/g-DCW), extracellular lysine was significantly increased when both *lysC*^{fbr} and *ybjE* were coexpressed (with extracellular:intracellular lysine ratios peaking at 138.7 and 197.2 for chromosomal and episomal expression, respectively). In contrast, when only one of either *lysC*^{fbr} or *ybjE* was expressed, this ratio reached a maximum of just 52.2 (i.e., when *ybjE* was expressed alone). For comparison, the control expressing neither gene achieved a ratio of 16.6 for lysine. Extracellular:intracellular ratios of aspartate followed an opposite trend to that of lysine, being reduced to minimum levels when *lysC*^{fbr} and *ybjE* were coexpressed (reaching just 2.5 and 3.4 for chromosomal and episomal expression, respectively), levels that remained similar to the empty vector control. Overall, *lysC*^{fbr} and *ybjE* coexpression were critical for lysine production in UTEX 2973, as significant flux to lysine was not possible without *LysC*^{fbr}, whereas the effective export of lysine was not possible without *YbjE*.

Engineering Direct Photosynthetic Production of Cadaverine. With a lysine overproducing strain of UTEX 2973 established, we next sought to leverage it as a platform for producing other, lysine-derived bioproducts. The first to be

https://doi.org/10.1021/acssynbio.1c00492
ACS Synth. Biol. 2021, 10, 3561−3575

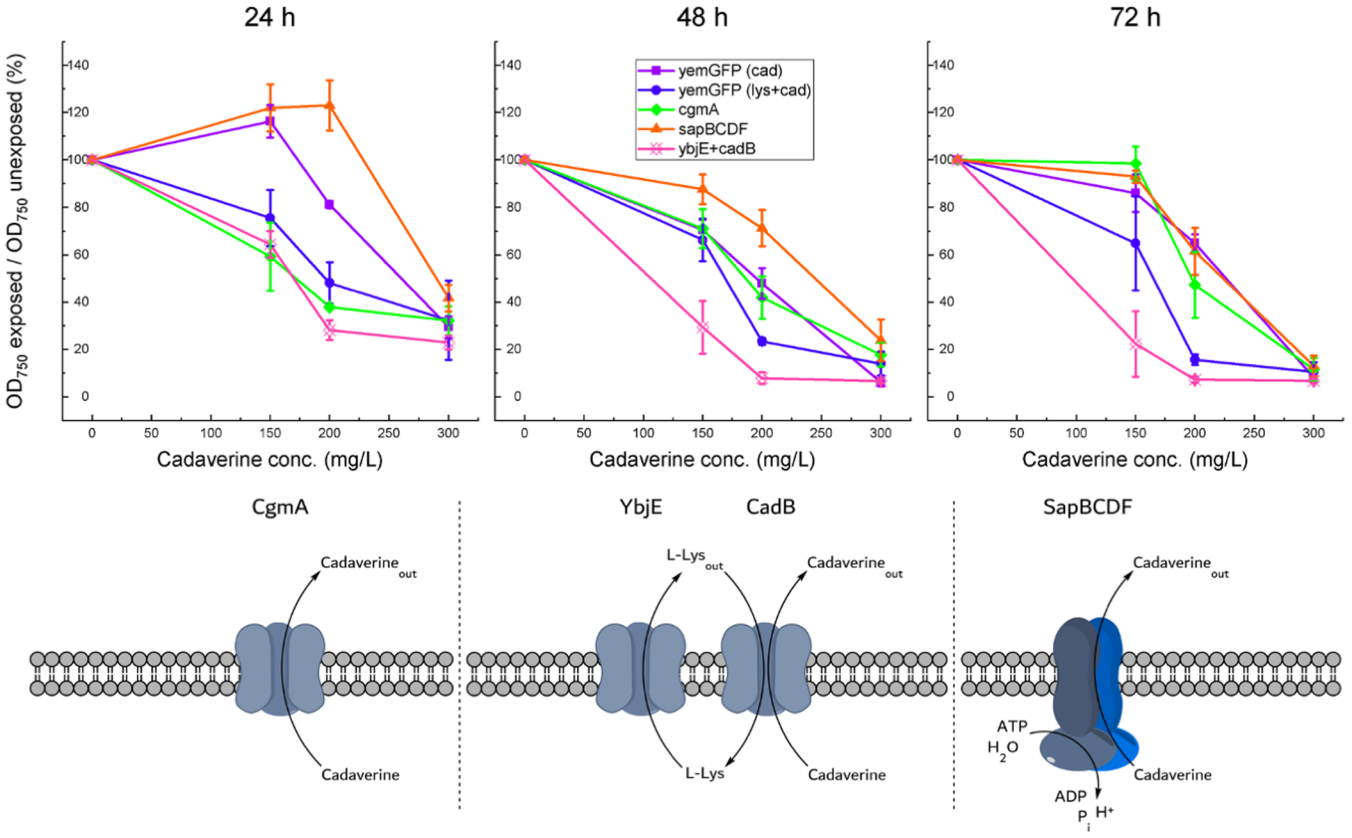

Figure 5. Comparison of exporter expression in UTEX 2973 in the presence of cadaverine. Above: comparing the growth of UTEX 2973 strains expressing different cadaverine export systems when exposed to increasing cadaverine concentrations versus unexposed. Tested exporters and controls were *yemGFP* in the presence of cadaverine (purple squares), *yemGFP* in the presence of both lysine and cadaverine (blue circles), *cgmA* in the presence of cadaverine (green diamonds), *sapBCDF* in the presence of cadaverine (orange triangles), and *ybjE* and *cadB* in the presence of cadaverine (pink bullseyes). Error bars represent standard error from biological triplicate. Below: modes of cadaverine export by each of the evaluated systems including (from left to right) CgmA, CadB with YbjE, and SapBCDF.

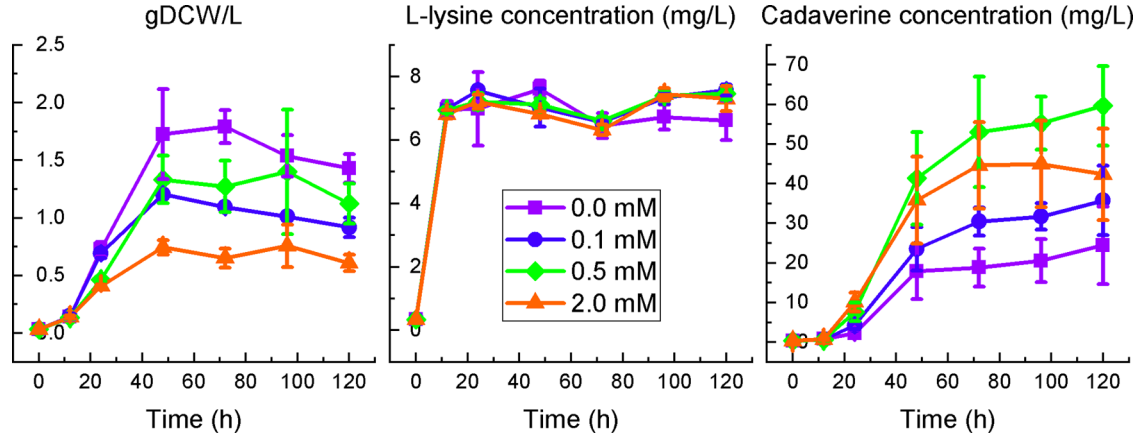

Figure 6. Cadaverine production by engineered UTEX 2973. Accumulation of biomass (left), lysine (middle), and cadaverine (right) for 120 h by UTEX 2973 harboring pZD-LGC-30 in shake flasks containing 25 mL BG-11 at varying concentrations of theophylline. Theophylline concentrations used were 0 mM (purple squares), 0.1 mM (blue circles), 0.5 mM (green diamonds), and 2.0 mM (orange triangles). Error bars represent standard error from biological triplicate.

targeted was cadaverine, a 5-carbon diamine with applications as a bioplastic monomer. However since cadaverine, unlike lysine, is not a native product, it was initially unclear (i) how well it would be tolerated by UTEX 2973 and (ii) if it could be effectively exported. Since active efflux can itself constitute an effective tolerance mechanism,[61−63] we first sought to address both prospective challenges by evaluating the heterologous function of a series of different cadaverine exporters and their impact on the ability of UTEX 2973 to tolerate exogenously supplied cadaverine over a range of concentrations (Figure 5). The specific exporters of interest included the cadaverine-exporting facilitator permease encoded by *cgmA* from *C. glutamicum*[64] (pZD-LGC-22) and the putrescine/cadaverine ABC transporter encoded by *sapBCDF* from *E. coli*[10,65] (pZD-

https://doi.org/10.1021/acssynbio.1c00492
ACS Synth. Biol. 2021, 10, 3561−3575

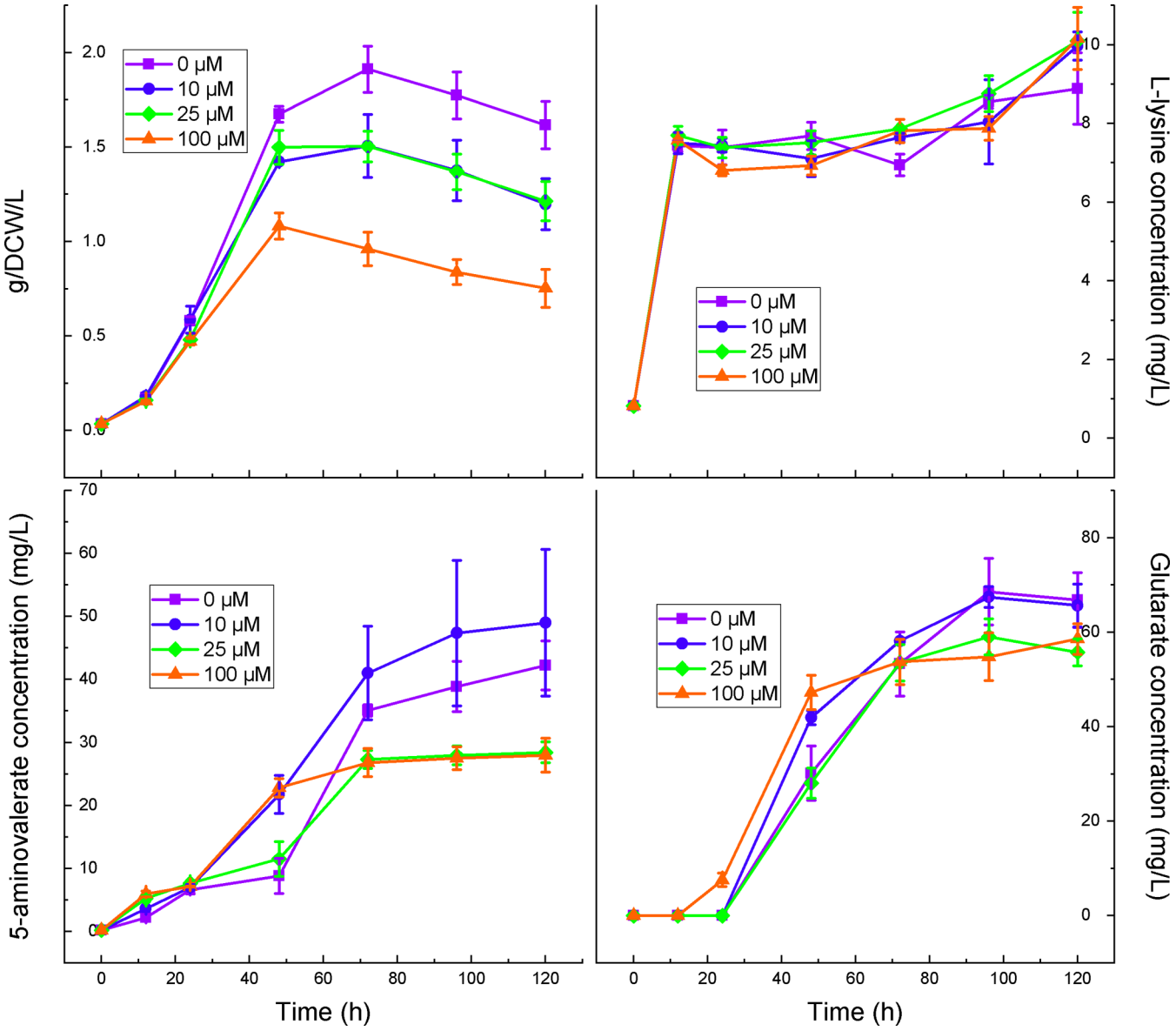

Figure 7. Glutarate production by engineered UTEX 2973. Accumulation of biomass (top left), lysine (top right), 5-AMV (bottom left), and glutarate (bottom right) by UTEX 2973 harboring pZD-LGC-32 in shake flasks containing 25 mL BG-11 at varying concentrations of IPTG. IPTG concentrations used were 0 μM (purple squares), 10 μM (blue circles), 25 μM (green diamonds), and 100 μM (orange triangles). Error bars represent standard error from biological triplicate.

LGC-23). Furthermore, the lysine:cadaverine antiporter encoded by *cadB* from *E. coli*[66] was also investigated, in this case by coexpressing it together with *ybjE* (pZD-LGC-27) while additionally supplementing the medium with 860 mg/L-lysine (twice the molar equivalent of the maximal cadaverine concentration used, i.e., 300 mg/L) to provide the biochemical driving force needed for cadaverine export. A control plasmid expressing *yemGFP* (pZD-LGC-02) was also constructed and used for comparison. In all cases, exposure to 300 mg/L cadaverine proved severe, with near-complete loss of growth (i.e., 75−85% reduction relative to the growth of the same strain at 0 mg/L cadaverine) within 48−72 h. Overall, while cadaverine was relatively toxic to UTEX 2973, strains expressing the *sapBCDF* generally displayed the highest tolerance, especially when faced with concentrations in the range of 150−200 mg/L. The *ybjE/cadB* antiporter, meanwhile, fared the worst, displaying poorer cadaverine tolerance than even the control strain, likely as a result of the increased burden associated with coexpressing two membrane proteins. Based on these outcomes, *sapBCDF* was selected to be advanced in support of engineering cadaverine biosynthesis.

To explore de novo cadaverine production by UTEX 2973, pZD-LGC-30 was next constructed to coexpress *lysC*^{fbr} (via P_{trc2O}-*lacI/O*), *cadA* (via P_{conII}−Riboswitch-F), and *sapBCDF* (via P_{cpcB1*}). Following conjugation, UTEX 2973 harboring pZD-LGC-30 was then cultivated in BG-11 media containing no IPTG and a range of theophylline concentrations. Here, as seen in Figure 6, while cadaverine production was possible in all cases, a maximum final titer of 59.7 ± 10.0 mg/L was achieved by 120 h when using 0.5 mM theophylline. Minor coaccumulation of lysine was also observed in all cultures (reaching ∼6−8 mg/L), though this behavior was consistent with the empty vector control (Figure S5) and remained insensitive to the *cadA* induction level. While providing no

https://doi.org/10.1021/acssynbio.1c00492
ACS Synth. Biol. 2021, 10, 3561−3575

Table 3. Comparing the Photosynthetic Production of Various Amino Acids and Bioplastic Monomers by Engineered Strains of Cyanobacteria

	product	host	conditions (CO_2, temp., LI)	final titer (mg/L)	product-to-biomass yield (mg/g-DCW)	productivity (mg/(L h))	duration (days)	reference
amino acids	L-lysine	UTEX 2973	1% CO_2, 38 °C, 200 $\mu E/(m^2\ s)$	556.3	349.1	4.64	5	this study
	L-lysine	PCC 7002	1% CO_2, 37 °C, 200 $\mu E/(m^2\ s)$	454.7	164.5	0.95	20	24
	L-phenylalanine	PCC 6803	3% CO_2, 30 °C, 50 $\mu E/(m^2\ s)$	579.8	904	2.42	10	72
	L-tyrosine	PCC 6803	3% CO_2, 30 °C, 50 $\mu E/(m^2\ s)$	41.1	64	0.17	10	72
	L-tryptophan	PCC 6803	3% CO_2, 30 °C, 240 $\mu E/(m^2\ s)$	212	57.5	0.88	10	73

	product	host	conditions (CO_2, temp., LI)	final titer (mg/L)	product-to-biomass yield (mg/g-DCW)	productivity (mg/(L h))	duration (days)	reference
bioplastic monomers	cadaverine	UTEX 2973	1% CO_2, 38 °C, 200 $\mu E/(m^2\ s)$	59.7	53.1	0.50	5	this study
	glutaric acid	UTEX 2973	1% CO_2, 38 °C, 200 $\mu E/(m^2\ s)$	68.6	38.7	0.71	4	this study
	3-hydroxybutyric acid	PCC 6803	Air, 30 °C, 120 $\mu E/(m^2\ s)$	533.4	nd	1.06	21	74
	3-hydroxypropionic acid	PCC 6803	Air, 30 °C, 50 $\mu E/(m^2\ s)$	837.2	359.3	5.81	6	38
	3-hydroxypropionic acid	PCC 7942	Air, 30 °C, 50 $\mu E/(m^2\ s)$	665	nd	2.31	12	75
	succinic acid	PCC 7942	Air, 30 °C, 30 $\mu E/(m^2\ s)$	430	nd	2.24	8	70
	L-lactic acid	PCC 6803	Air, 30 °C, 100 $\mu E/(m^2\ s)$	1140	nd	1.58	30	76
	L-lactic acid	PCC 6803	Air, 30 °C, 30 $\mu E/(m^2\ s)$	288.3	34.1	0.71	17	77
	L-lactic acid	PCC 7942	Air, 30 °C, 18h L/6h D	56.3	nd	0.59	4	44
	ethylene	PCC 6803	5% CO_2, 30 °C, 50 $\mu E/(m^2\ s)$	342	nd	7.125	2	78

theophylline led to the best growth (reaching up to 1.79 ± 0.14 g-DCW/L), this also resulted in the lowest final cadaverine titers (24.4 ± 9.8 mg/L). It should also be noted that, although no proteomic analysis was performed to confirm the expression of the pathway genes, no cadaverine was detected for 120 h for either wild-type UTEX 2973 or the lysine-producing strain (i.e., carrying pZD-LGC-13; not shown). In general, when compared with the lysine-producing strains, fitness losses displayed during cadaverine production were of a similar magnitude as those displayed by the lysine control strain expressing just $lysC^{fbr}$ alone (i.e., no *ybjE*; Figure 3G). This could suggest that fitness losses during cadaverine production were again a result of intracellular lysine build-up, as would be caused in this case by its inefficient conversion to and/or export of cadaverine. That said, a further increase in *cadA* expression (i.e., using 2 mM theophylline) led to reduced cadaverine production (45.0 ± 10.9 mg/L) along with an even greater decline in fitness (with the maximum biomass concentration reaching just 0.76 ± 0.18 g-DCW/L; Figure 6). Thus, it appears most likely that the fitness defect, in this case, was instead due to inefficient cadaverine export, which, in turn, may have caused a metabolite "backlog" that, due to intracellular lysine and/or cadaverine accumulation, led to growth inhibition. Indeed, the extracellular:intracellular cadaverine ratio was found to be 2.6 times higher when using 2.0 mM theophylline (i.e., stronger *cadA* expression) relative to 0.5 mM theophylline (13.1 vs 34.7; Figure S6). Further engineering of an effective cadaverine exporter and/or optimization of its expression is therefore expected to be critical for future improvements in photosynthetic cadaverine production.

Engineering Direct Photosynthetic Production of Glutarate. To further explore the photosynthetic production of lysine-derived biochemicals, we lastly engineered UTEX 2973 to produce glutarate via an alternative extension of the lysine pathway. Like cadaverine, the 5-carbon dicarboxylate glutarate is also of interest for bioplastic production. As previously demonstrated in other hosts,[8−10,67] glutarate can be produced from lysine via the intermediate 5-aminovalerate (5-AMV) using the *davBA* and *davDT* operons from *P. putida*.[68,69] Although glutarate has not previously been produced by cyanobacteria, its 4-carbon analogue succinate has. Specifically, Lan and Wei showed that succinate could be overproduced by PCC 7942 without any apparent inhibitory effects and also that it was naturally secreted (although the associated secretion mechanism remains unclear).[69] Considering its structural similarity with succinate, we postulated that the same might also hold true for glutarate. Accordingly, plasmid pZD-LGC-32 was constructed, where, in place of *ybjE* on pZD-LGC-13, an expression cassette including both the *davBA* and *davDT* operons were included. As with cadaverine production, glutarate was not detected for 120 h for either wild-type UTEX 2973 or the lysine-producing strain (i.e., carrying pZD-LGC-13; not shown). In contrast, carrying pZD-LGC-32, UTEX 2973 was found to produce glutarate at a maximum titer of 68.6 ± 7.1 mg/L by 96 h (Figure 7). Meanwhile, as was the case for cadaverine production, in the absence of *ybjE* expression, extracellular lysine accumulation

https://doi.org/10.1021/acssynbio.1c00492
ACS Synth. Biol. 2021, 10, 3561−3575

was modest and again ~8 mg/L. Similar to lysine production under the expression of pZD-LGC-13, leaky expression of $lysC^{fbr}$ (i.e., 0 μM IPTG) still resulted in significant glutarate production, whereas cell growth was again reduced with increasing IPTG concentrations (also like lysine production; Figure 3D). Overall, glutarate production proved largely insensitive to the IPTG induction level, suggesting that the current flux bottleneck likely resides downstream of aspartate kinase. Notably, as seen in Figure 7, 5-AMV accumulated to higher levels at lower IPTG concentrations (conditions promoting greater lysine production), an outcome that implicates inefficient glutarate export and/or suboptimal expression of the *davDT* operon as the most probable bottlenecks. Future work should investigate such prospects to improve photosynthetic glutarate production.

DISCUSSION

In this study, we first demonstrate the systematic engineering of fast-growing UTEX 2973 for the photosynthetic production of lysine. In addition to lysine, multiple other examples of cyanobacterial amino acid production have also been reported. As seen in Table 3, while such demonstrations using UTEX 2973 have so far been limited, its fast-growing phenotype appears to provide a productivity benefit with respect to amino acid biosynthesis, an outcome that should be extended to and validated for other products. While efforts to improve lysine production by increasing flux to OAA were ultimately unsuccessful here, this result stands in stark contrast to prior reports. Notably, while investigating photoautotrophic succinic acid production by PCC 7942, Lan and Wei[70] reported a roughly 3.6-fold improvement in the final titer along with a 4-fold improvement in the final biomass when expressing phosphoenolpyruvate carboxylase (in this case together with *E. coli gltA* encoding citrate synthase). Thus, this approach should not be fully discredited with respect to improving lysine production by UTEX 2973; however, more thorough optimization will likely be critical in this regard. Whereas the optimization of $lysC^{fbr}$ expression was important to maximizing lysine production in this study, following this, the most significant performance improvements were realized as a result of episomally expressing the key pathway genes. Although gene dosage effects are routinely exploited in heterotrophs like *E. coli*, this remains a largely underexplored design parameter with respect to metabolic engineering in most cyanobacteria. Therefore, the further development of diverse and versatile shuttle vector systems will likely also be useful for enhancing other metabolic engineering efforts in cyanobacteria.

Following lysine production, this work also demonstrated how, through a modular pathway engineering approach, cyanobacteria could be further engineered to produce cadaverine and glutarate—two bioplastic monomer compounds that, to the best of our knowledge, have not before been synthesized photosynthetically. Similar to lysine, however, there are many examples of the heterotrophic bioproduction of these two compounds. For example, recent work in *E. coli* has demonstrated glutarate production at up to 54.5 g/L using a unique engineered pathway in which cadaverine serves as an intermediate.[71] *C. glutamicum*, meanwhile, has been engineered to produce glutarate at up to a remarkable 105.3 g/L over the course of just 69 h.[55] The maximum cadaverine titer reported in *C. glutamicum* is similar, reaching up to 103.8 g/L after 65 h.[7] Although the photoautotrophic performance achieved here remains orders of magnitude lower, our work also highlights several challenges common to both photoautotrophs and heterotrophs alike, including the cruciality of relieving intermediate accumulation and efficiently exporting final products to affect efficient bioproduction.[55,67,71] While photosynthetic cadaverine and glutarate titers thus far remain low compared with many other monomer compounds so far synthesized by cyanobacteria, they do uniquely represent among the only 5-carbon molecules investigated to date. As seen in Table 3, it could be inferred that shorter-chain monomers are more easily produced by cyanobacteria, which is perhaps a result of their improved export.[44] The outcomes of this study do indeed suggest that the future discovery/engineering of effective transporters for cadaverine and glutarate may ultimately be critical to future enhancements in their production by UTEX 2973.

ASSOCIATED CONTENT

Supporting Information

The Supporting Information is available free of charge at https://pubs.acs.org/doi/10.1021/acssynbio.1c00492.

Growth profile of wild-type UTEX 2973 under standard conditions; calibration developed and used to correlate biomass measurements in OD_{750} with g-DCW/L; comparison of plates containing UTEX 2973 exconjugants; comparison of the influence of different strategies for increasing flux to OAA during L-lysine production by UTEX 2973; extracellular accumulation of L-aspartate and L-lysine by UTEX 2973 harboring pZD-LGC-04; comparison of intracellular vs extracellular accumulation of cadaverine by engineered UTEX 2973; and a list of primers designed for and used in this study for plasmid construction, colony PCR, and sequencing (PDF)

AUTHOR INFORMATION

Corresponding Author

David R. Nielsen − *Chemical Engineering, School for Engineering of Matter, Transport, and Energy, Arizona State University, Tempe, Arizona 85287-6106, United States;* orcid.org/0000-0002-9310-2000; Phone: (480) 965-4113; Email: David.R.Nielsen@asu.edu; Fax: (480) 727-9321

Author

Zachary A. Dookeran − *Chemical Engineering, School for Engineering of Matter, Transport, and Energy, Arizona State University, Tempe, Arizona 85287-6106, United States*

Complete contact information is available at: https://pubs.acs.org/10.1021/acssynbio.1c00492

Author Contributions

Z.A.D. and D.R.N. conceived the idea, designed the experiments, and wrote the manuscript. Z.A.D. conducted and analyzed all experiments.

Notes

The authors declare no competing financial interest.

ACKNOWLEDGMENTS

This work was conducted with support from the National Science Foundation (CBET-1705409). The authors declare no commercial or financial conflict of interest associated with the content of this manuscript.

REFERENCES

(1) Hoffmann, S. L.; Jungmann, L.; Schiefelbein, S.; Peyriga, L.; Cahoreau, E.; Portais, J. C.; Becker, J.; Wittmann, C. Lysine production from the sugar alcohol mannitol: Design of the cell factory *Corynebacterium glutamicum* SEA-3 through integrated analysis and engineering of metabolic pathway fluxes. *Metab. Eng.* **2018**, *47*, 475−487.

(2) Eggeling, L.; Bott, M. A giant market and a powerful metabolism: L-lysine provided by *Corynebacterium glutamicum*. *Appl. Microbiol. Biotechnol.* **2015**, *99*, 3387−3394.

(3) Koffas, M.; Stephanopoulos, G. Strain improvement by metabolic engineering: Lysine production as a case study for systems biology. *Curr. Opin. Biotechnol.* **2005**, *16*, 361−366.

(4) Wittmann, C.; Becker, J. The L-Lysine Story: From Metabolic Pathways to Industrial Production. In *Amino Acid Biosynthesis—Pathways, Regulation and Metabolic Engineering*; Wendisch, V. F., Ed.; Springer: Berlin, Heidelberg, 2007.

(5) Mimitsuka, T.; Sawai, H.; Hatsu, M.; Yamada, K. Metabolic engineering of *Corynebacterium glutamicum* for cadaverine fermentation. *Biosci., Biotechnol., Biochem.*. **2007**, *71*, 2130−2135.

(6) Tateno, T.; Okada, Y.; Tsuchidate, T.; Tanaka, T.; Fukuda, H.; Kondo, A. Direct production of cadaverine from soluble starch using *Corynebacterium glutamicum* coexpressing α-amylase and lysine decarboxylase. *Appl. Microbiol. Biotechnol.* **2009**, *82*, 115−121.

(7) Kim, H. T.; Baritugo, K. A.; Oh, Y. H.; Hyun, S. M.; Khang, T. U.; Kang, K. H.; Jung, S. H.; Song, B. K.; Park, K.; Kim, I. K.; Lee, M. O.; Kam, Y.; Hwang, Y. T.; Park, S. J.; Joo, J. C. Metabolic engineering of *Corynebacterium glutamicum* for the high-level production of cadaverine that can be used for the synthesis of Biopolyamide 510. *ACS Sustainable Chem. Eng.* **2018**, *6*, 5296−5305.

(8) Adkins, J.; Jordan, J.; Nielsen, D. R. Engineering *Escherichia coli* for renewable production of the 5-carbon polyamide building-blocks 5-aminovalerate and glutarate. *Biotechnol. Bioeng.* **2013**, *110*, 1726−1734.

(9) Park, S. J.; Kim, E. Y.; Noh, W.; Park, H. M.; Oh, Y. H.; Lee, S. H.; Song, B. K.; Jegal, J.; Lee, S. Y. Metabolic engineering of *Escherichia coli* for the production of 5-aminovalerate and glutarate as C5 platform chemicals. *Metab. Eng.* **2013**, *16*, 42−47.

(10) Li, W.; Ma, L.; Shen, X.; Wang, J.; Feng, Q.; Liu, L.; Zheng, G.; Yan, Y.; Sun, X.; Yuan, Q. Targeting metabolic driving and intermediate influx in lysine catabolism for high-level glutarate production. *Nat. Commun.* **2019**, *10*, No. 3337.

(11) Kinoshita, S.; Udaka, S.; Shimono, M. Studies on the amino acid fermentation Part 1. Production of L-glutamic acid by various microorganisms. *J. Gen. Appl. Microbiol.* **1957**, *3*, 193−205.

(12) Ikeda, M. Amino Acid Production Processes. In *Microbial Production of L-Amino Acids*; Faurie, R.; Thommel, J.; Bathe, B.; Debabov, V. G.; Huebner, S.; Ikeda, M.; Kimura, E.; Marx, A.; Mockel, B.; Mueller, U.; Pfefferle, W., Eds.; Springer: Berlin, Heidelberg, 2003.

(13) Becker, J.; Zelder, O.; Häfner, S.; Schröder, H.; Wittmann, C. From zero to hero-Design-based systems metabolic engineering of *Corynebacterium glutamicum* for L-lysine production. *Metab. Eng.* **2011**, *13*, 159−168.

(14) Xu, J.; Han, M.; Zhang, J.; Guo, Y.; Zhang, W. Metabolic engineering *Corynebacterium glutamicum* for the L-lysine production by increasing the flux into L-lysine biosynthetic pathway. *Amino Acids* **2014**, *46*, 2165−2175.

(15) van Ooyen, J.; Noack, S.; Bott, M.; Reth, A.; Eggeling, L. Improved L-lysine production with *Corynebacterium glutamicum* and systemic insight into citrate synthase flux and activity. *Biotechnol. Bioeng.* **2012**, *109*, 2070−2081.

(16) Kind, S.; Becker, J.; Wittmann, C. Increased lysine production by flux coupling of the tricarboxylic acid cycle and the lysine biosynthetic pathway-Metabolic engineering of the availability of succinyl-CoA in *Corynebacterium glutamicum*. *Metab. Eng.* **2013**, *15*, 184−195.

(17) Bommareddy, R. R.; Chen, Z.; Rappert, S.; Zeng, A. P. A de novo NADPH generation pathway for improving lysine production of *Corynebacterium glutamicum* by rational design of the coenzyme specificity of glyceraldehyde 3-phosphate dehydrogenase. *Metab. Eng.* **2014**, *25*, 30−37.

(18) Buchholz, J.; Schwentner, A.; Brunnenkan, B.; Gabris, C.; Grimm, S.; Gerstmeir, R.; Takors, R.; Eikmanns, B. J.; Blombacha, B. Platform engineering of *Corynebacterium glutamicum* with reduced pyruvate dehydrogenase complex activity for improved production of L-lysine, L-valine, and 2-ketoisovalerate. *Appl. Environ. Microbiol.* **2013**, *79*, 5566−5575.

(19) Xu, J. Z.; Ruan, H. Z.; Yu, H. B.; Liu, L. M.; Zhang, W. Metabolic engineering of carbohydrate metabolism systems in *Corynebacterium glutamicum* for improving the efficiency of L-lysine production from mixed sugar. *Microb. Cell Fact.* **2020**, *19*, No. 39.

(20) Buschke, N.; Schröder, H.; Wittmann, C. Metabolic engineering of *Corynebacterium glutamicum* for production of 1,5-diaminopentane from hemicellulose. *Biotechnol. J.* **2011**, *6*, 306−317.

(21) Gopinath, V.; Meiswinkel, T. M.; Wendisch, V. F.; Nampoothiri, K. M. Amino acid production from rice straw and wheat bran hydrolysates by recombinant pentose-utilizing *Corynebacterium glutamicum*. *Appl. Microbiol. Biotechnol.* **2011**, *92*, 985−996.

(22) Kawaguchi, H.; Sasaki, M.; Vertès, A. A.; Inui, M.; Yukawa, H. Engineering of an L-arabinose metabolic pathway in *Corynebacterium glutamicum*. *Appl. Microbiol. Biotechnol.* **2008**, *77*, 1053−1062.

(23) Sasaki, M.; Jojima, T.; Inui, M.; Yukawa, H. Simultaneous utilization of d-cellobiose, d-glucose, and d-xylose by recombinant *Corynebacterium glutamicum* under oxygen-deprived conditions. *Appl. Microbiol. Biotechnol.* **2008**, *81*, 691−699.

(24) Korosh, T. C.; Markley, A. L.; Clark, R. L.; McGinley, L. L.; McMahon, K. D.; Pfleger, B. F. Engineering photosynthetic production of L-lysine. *Metab. Eng.* **2017**, *44*, 273−283.

(25) Yu, J.; Liberton, M.; Cliften, P. F.; Head, R. D.; Jacobs, J. M.; Smith, R. D.; Koppenaal, D. W.; Brand, J. J.; Pakrasi, H. B. *Synechococcus elongatus* UTEX 2973, a fast growing cyanobacterial chassis for biosynthesis using light and CO_2. *Sci. Rep.* **2015**, *5*, No. 8132.

(26) Ungerer, J.; Lin, P. C.; Chen, H. Y.; Pakrasi, H. B. Adjustments to photosystem stoichiometry and electron transfer proteins are key to the remarkably fast growth of the Cyanobacterium *Synechococcus elongatus* UTEX 2973. *mBio* **2018**, *9*, 1−12.

(27) Knoot, C. J.; Khatri, Y.; Hohlman, R. M.; Sherman, D. H.; Pakrasi, H. B. Engineered production of hapalindole alkaloids in the cyanobacterium *Synechococcus* sp. UTEX 2973. *ACS Synth. Biol.* **2019**, *8*, 1941−1951.

(28) Song, K.; Tan, X.; Liang, Y.; Lu, X. The potential of *Synechococcus elongatus* UTEX 2973 for sugar feedstock production. *Appl. Microbiol. Biotechnol.* **2016**, *100*, 7865−7875.

(29) Lin, P. C.; Zhang, F.; Pakrasi, H. B. Enhanced production of sucrose in the fast-growing cyanobacterium *Synechococcus elongatus* UTEX 2973. *Sci. Rep.* **2020**, *10*, No. 390.

(30) Lin, P. C.; Zhang, F.; Pakrasi, H. B. Enhanced limonene production in a fast-growing cyanobacterium through combinatorial metabolic engineering. *Metab. Eng. Commun.* **2021**, *12*, No. e00164.

(31) Gibson, D. G.; Young, L.; Chuang, R. Y.; Venter, J. C.; Hutchison, C. A.; Smith, H. O. Enzymatic assembly of DNA molecules up to several hundred kilobases. *Nat. Methods* **2009**, *6*, 343−345.

(32) Liu, D.; Pakrasi, H. B. Exploring native genetic elements as plug-in tools for synthetic biology in the cyanobacterium *Synechocystis* sp. PCC 6803. *Microb. Cell Fact.* **2018**, *17*, No. 48.

(33) Jones, C. M.; Korosh, T. C.; Nielsen, D. R.; Pfleger, B. F. Optimization of a T7-RNA polymerase system in *Synechococcus* sp. PCC 7002 mirrors the protein overproduction phenotype from *E. coli* BL21(DE3). *Appl. Microbiol. Biotechnol.* **2021**, *105*, 1147−1158.

(34) Chen, Y.; Taton, A.; Go, M.; London, R. E.; Pieper, L. M.; Golden, S. S.; Golden, J. W. Self-replicating shuttle vectors based on pANS, a small endogenous plasmid of the unicellular cyanobacterium *Synechococcus elongatus* PCC 7942. *Microbiology* **2016**, *162*, 2029−2041.

https://doi.org/10.1021/acssynbio.1c00492
ACS Synth. Biol. 2021, 10, 3561−3575

(35) Englund, E.; Andersen-Ranberg, J.; Miao, R.; Hamberger, B.; Lindberg, P. Metabolic engineering of *Synechocystis* sp. PCC 6803 for production of the plant diterpenoid manoyl oxide. *ACS Synth. Biol.* **2015**, *4*, 1270−1278.
(36) Kim, Y. H.; Kim, H. J.; Shin, J. H.; Bhatia, S. K.; Seo, H. M.; Kim, Y. G.; Lee, Y. K.; Yang, Y. H.; Park, K. Application of diethyl ethoxymethylenemalonate (DEEMM) derivatization for monitoring of lysine decarboxylase activity. *J. Mol. Catal. B: Enzym.* **2015**, *115*, 151−154.
(37) Li, S.; Sun, T.; Xu, C.; Chen, L.; Zhang, W. Development and optimization of genetic toolboxes for a fast-growing cyanobacterium *Synechococcus elongatus* UTEX 2973. *Metab. Eng.* **2018**, *48*, 163−174.
(38) Wang, X.; Liu, W.; Xin, C.; Zheng, Y.; Cheng, Y.; Sun, S.; Li, R.; Zhu, X. G.; Dai, S. Y.; Rentzepis, P. M.; Yuan, J. S. Enhanced limonene production in cyanobacteria reveals photosynthesis limitations. *Proc. Natl. Acad. Sci. U.S.A.* **2016**, *113*, 14225−14230.
(39) Kulkarni, R. D.; Golden, S. S. mRNA stability is regulated by a coding-region element and the unique 5′ untranslated leader sequences of the three *Synechococcus psba* transcripts. *Mol. Microbiol.* **1997**, *24*, 1131−1142.
(40) Andersson, C. R.; Tsinoremas, N. F.; Shelton, J.; Lebedeva, N.; Yarrow, J.; Min, H.; Golden, S. S. Application of bioluminescence to the study of circadian rhythms in cyanobacteria. *Methods Enzymol.* **2000**, *305*, 527−542.
(41) Mileyko, Y.; Joh, R. I.; Weitz, J. S. Small-scale copy number variation and large-scale changes in gene expression. *Proc. Natl. Acad. Sci. U.S.A.* **2008**, *105*, 16659−16664.
(42) Kittleson, J. T.; Wu, G. C.; Anderson, J. C. Successes and failures in modular genetic engineering. *Curr. Opin. Chem. Biol.* **2012**, *16*, 329−336.
(43) Segall-Shapiro, T. H.; Sontag, E. D.; Voigt, C. A. Engineered promoters enable constant gene expression at any copy number in bacteria. *Nat. Biotechnol.* **2018**, *36*, 352−358.
(44) Niederholtmeyer, H.; Wolfstädter, B. T.; Savage, D. F.; Silver, P. A.; Way, J. C. Engineering cyanobacteria to synthesize and export hydrophilic products. *Appl. Environ. Microbiol.* **2010**, *76*, 3462−3466.
(45) Topp, S.; Reynoso, C. M. K.; Seeliger, J. C.; Goldlust, I. S.; Desai, S. K.; Murat, D.; Shen, A.; Puri, A. W.; Komeili, A.; Bertozzi, C. R.; Scott, J. R.; Gallivan, J. P. Synthetic riboswitches that induce gene expression in diverse bacterial species. *Appl. Environ. Microbiol.* **2010**, *76*, 7881−7884.
(46) Nakahira, Y.; Ogawa, A.; Asano, H.; Oyama, T.; Tozawa, Y. Theophylline-dependent riboswitch as a novel genetic tool for strict regulation of protein expression in cyanobacterium *Synechococcus elongatus* PCC 7942. *Plant Cell Physiol.* **2013**, *54*, 1724−1735.
(47) Ma, A. T.; Schmidt, C. M.; Golden, J. W. Regulation of gene expression in diverse cyanobacterial species by using theophylline-responsive riboswitches. *Appl. Environ. Microbiol.* **2014**, *80*, 6704−6713.
(48) Steinhauser, D.; Fernie, A. R.; Araújo, W. L. Unusual cyanobacterial TCA cycles: Not broken just different. *Trends Plant Sci.* **2012**, *17*, 503−509.
(49) Schwarz, D.; Nodop, A.; Hüge, J.; Purfürst, S.; Forchhammer, K.; Michel, K. P.; Bauwe, H.; Kopka, J.; Hagemann, M. Metabolic and transcriptomic phenotyping of inorganic carbon acclimation in the cyanobacterium *Synechococcus elongatus* PCC 7942. *Plant Physiol.* **2011**, *155*, 1640−1655.
(50) Ciebiada, M.; Kubiak, K.; Daroch, M. Modifying the cyanobacterial metabolism as a key to efficient biopolymer production in photosynthetic microorganisms. *Int. J. Mol. Sci.* **2020**, *21*, No. 7204.
(51) Xiong, W.; Brune, D.; Vermaas, W. F. J. The γ-aminobutyric acid shunt contributes to closing the tricarboxylic acid cycle in *Synechocystis* sp. PCC 6803. *Mol. Microbiol.* **2014**, *93*, 786−796.
(52) Zhang, S.; Bryant, D. A. The tricarboxylic acid cycle in cyanobacteria. *Science* **2011**, *334*, 1551−1553.
(53) Zhang, S.; Qian, X.; Chang, S.; Dismukes, G. C.; Bryant, D. A. Natural and synthetic variants of the tricarboxylic acid cycle in cyanobacteria: Introduction of the GABA shunt into *Synechococcus* sp. PCC 7002. *Front. Microbiol.* **2016**, *7*, No. 1972.
(54) Abernathy, M. H.; Yu, J.; Ma, F.; Liberton, M.; Ungerer, J.; Hollinshead, W. D.; Gopalakrishnan, S.; He, L.; Maranas, C. D.; Pakrasi, H. B.; Allen, D. K.; Tang, Y. J. Deciphering cyanobacterial phenotypes for fast photoautotrophic growth via isotopically nonstationary metabolic flux analysis. *Biotechnol. Biofuels* **2017**, *10*, No. 273.
(55) Han, T.; Kim, G. B.; Lee, S. Y. Glutaric acid production by systems metabolic engineering of an L-lysine−overproducing *Corynebacterium glutamicum*. *Proc. Natl. Acad. Sci. U.S.A.* **2020**, *117*, 30328−30334.
(56) Pathania, A.; Sardesai, A. A. Distinct paths for basic amino acid export in *Escherichia coli*: YbjE (LysO) mediates export of L-lysine. *J. Bacteriol.* **2015**, *197*, 2036−2047.
(57) Bellmann, A.; Vrljić, M.; Pátek, M.; Sahm, H.; Krämer, R.; Eggeling, L. Expression control and specificity of the basic amino acid exporter *lysE* of *Corynebacterium glutamicum*. *Microbiology* **2001**, *147*, 1765−1774.
(58) Vrljic, M.; Garg, J.; Bellmann, A.; Wachi, S.; Freudl, R.; Malecki, M. J.; Sahm, H.; Kozina, V. J.; Eggeling, L.; Saier, M. H. The LysE superfamily: Topology of the lysine exporter LysE of *Corynebacterium glutamicum*, a paradyme for a novel superfamily of transmembrane solute translocators. *J. Mol. Microbiol. Biotechnol.* **1999**, *1*, 327−336.
(59) Vrljic, M.; Sahm, H.; Eggeling, L. A new type of transporter with a new type of cellular function: L-lysine export from *Corynebacterium glutamicum*. *Mol. Microbiol.* **1996**, *22*, 815−826.
(60) Malla, S.; van der Helm, E.; Darbani, B.; Wieschalka, S.; Forster, J.; Borodina, I.; Sommer, M. *A Novel Efficient L-lysine Exporter Identified by Functional Metagenomics*; bioRxiv, 2020.
(61) Onyeabor, M.; Martinez, R.; Kurgan, G.; Wang, X. Engineering Transport Systems for Microbial Production. In *Advances in Applied Microbiology*, 1st ed.; Gadd, G.; Sariaslani, S., Eds.; Elsevier: USA, 2020; Vol. *111*.
(62) Machas, M.; Kurgan, G.; Jha, A. K.; Flores, A.; Schneider, A.; Coyle, S.; Varman, A. M.; Wang, X.; Nielsen, D. R. Emerging tools, enabling technologies, and future opportunities for the bioproduction of aromatic chemicals. *J. Chem. Technol. Biotechnol.* **2019**, *94*, 38−52.
(63) Mukhopadhyay, A. Tolerance engineering in bacteria for the production of advanced biofuels and chemicals. *Trends Microbiol.* **2015**, *23*, 498−508.
(64) Kind, S.; Kreye, S.; Wittmann, C. Metabolic engineering of cellular transport for overproduction of the platform chemical 1,5-diaminopentane in *Corynebacterium glutamicum*. *Metab. Eng.* **2011**, *13*, 617−627.
(65) Sugiyama, Y.; Nakamura, A.; Matsumoto, M.; Kanbe, A.; Sakanaka, M.; Higashi, K.; Igarashi, K.; Katayama, T.; Suzuki, H.; Kurihara, S. A novel putrescine exporter SapBCDF of *Escherichia coli*. *J. Biol. Chem.* **2016**, *291*, 26343−26351.
(66) Kanjee, U.; Houry, W. A. Mechanisms of acid resistance in *Escherichia coli*. *Annu. Rev. Microbiol.* **2013**, *67*, 65−68.
(67) Rohles, C. M.; Gießelmann, G.; Kohlstedt, M.; Wittmann, C.; Becker, J. Systems metabolic engineering of *Corynebacterium glutamicum* for the production of the carbon-5 platform chemicals 5-aminovalerate and glutarate. *Microb. Cell Fact.* **2016**, *15*, 1−13.
(68) Revelles, O.; Espinosa-Urgel, M.; Molin, S.; Ramos, J. L. The *davDT* operon of *Pseudomonas putida*, involved in lysine catabolism, is induced in response to the pathway intermediate δ-aminovaleric acid. *J. Bacteriol.* **2004**, *186*, 3439−3446.
(69) Revelles, O.; Espinosa-Urgel, M.; Fuhrer, T.; Sauer, U.; Ramos, J. L. Multiple and interconnected pathways for l-lysine catabolism in *Pseudomonas putida* KT2440. *J. Bacteriol.* **2005**, *187*, 7500−7510.
(70) Lan, E. I.; Wei, C. T. Metabolic engineering of cyanobacteria for the photosynthetic production of succinate. *Metab. Eng.* **2016**, *38*, 483−493.
(71) Li, W.; Ma, L.; Shen, X.; Wang, J.; Feng, Q.; Liu, L.; Zheng, G.; Yan, Y.; Sun, X.; Yuan, Q. Targeting metabolic driving and intermediate influx in lysine catabolism for high-level glutarate production. *Nat. Commun.* **2019**, *10*, No. 3337.
(72) Brey, L. F.; Włodarczyk, A. J.; Bang Thøfner, J. F.; Burow, M.; Crocoll, C.; Nielsen, I.; Zygadlo Nielsen, A. J.; Jensen, P. E. Metabolic

engineering of *Synechocystis* sp. PCC 6803 for the production of aromatic amino acids and derived phenylpropanoids. *Metab. Eng.* **2020**, *57*, 129−139.
(73) Deshpande, A.; Vue, J.; Morgan, J. Combining random mutagenesis and metabolic engineering for enhanced tryptophan production in *Synechocystis* sp. Strain PCC 6803. *Appl. Environ. Microbiol.* **2020**, *86*, No. e02816-19.
(74) Wang, B.; Pugh, S.; Nielsen, D. R.; Zhang, W.; Meldrum, D. R. Engineering cyanobacteria for photosynthetic production of 3-hydroxybutyrate directly from CO_2. *Metab. Eng.* **2013**, *16*, 68−77.
(75) Lan, E. I.; Chuang, D. S.; Shen, C. R.; Lee, A. M.; Ro, S. Y.; Liao, J. C. Metabolic engineering of cyanobacteria for photosynthetic 3-hydroxypropionic acid production from CO_2 using *Synechococcus elongatus* PCC 7942. *Metab. Eng.* **2015**, *31*, 163−170.
(76) Varman, A. M.; Yu, Y.; You, L.; Tang, Y. J. Photoautotrophic production of D-lactic acid in an engineered cyanobacterium. *Microb. Cell Fact.* **2013**, *12*, No. 117.
(77) Angermayr, S. A.; Paszota, M.; Hellingwerf, K. J. Engineering a cyanobacterial cell factory for production of lactic acid. *Appl. Environ. Microbiol.* **2012**, *78*, 7098−7106.
(78) Ungerer, J.; Tao, L.; Davis, M.; Ghirardi, M.; Maness, P. C.; Yu, J. Sustained photosynthetic conversion of CO_2 to ethylene in recombinant cyanobacterium *Synechocystis* 6803. *Energy Environ. Sci.* **2012**, *5*, 8998−9006.

https://doi.org/10.1021/acssynbio.1c00492
ACS Synth. Biol. 2021, 10, 3561−3575